Diffusion Tensor Imaging Tractography Parameters of Limbic System Bundles in Temporal Lobe Epilepsy Patients

Despina Liacu, Ilana Idy-Peretti, Denis Ducreux, Viviane Bouilleret, Giovanni de Marco

HAL Id: hal-01467723

https://hal.parisnanterre.fr/hal-01467723

Submitted on 10 Oct 2019

Diffusion Tensor Imaging Tractography Parameters of Limbic System Bundles in Temporal Lobe Epilepsy Patients

Despina Liacu, PhD,[1]* Ilana Idy-Peretti, MD, PhD,[2] Denis Ducreux, MD, PhD,[1] Viviane Bouilleret, MD,[3] and Giovanni de Marco, PhD[4]

Purpose: To investigate changes in diffusion tensor imaging (DTI) measures in limbic system white matter of patients with temporal lobe epilepsy (TLE) using diffusion tensor tractography.

Materials and Methods: DTI metrics including fractional anisotropy (FA), $\lambda 1$, $\lambda 2$, $\lambda 3$, and trace (Tr) coefficients were obtained from tractography for bilateral fornix, superior and inferior cingulum fibers in 18 patients and 10 healthy controls. Hippocampal signal-to-noise ratio (SNR) quantitative analysis was performed in order to confirm the magnetic resonance imaging (MRI) hippocampal lesion presence or absence in TLE patients.

Results: Nine patients presented unilateral hippocampal sclerosis (TLE+HS) and nine patients had no signal abnormalities on conventional MRI (TLE−HS). On the ipsilateral seizure side, all three investigated tracts showed significant DTI indices abnormalities in both patient groups when compared with controls, most marked on the inferior cingulum. Contralateral to the seizure side, the three tracts presented significant DTI parameters in only the TLE+HS group when compared with controls.

Conclusion: The DTI abnormalities found in the TLE−HS group may suggest that in the inferior cingulum the structural integrity is more affected than in the fornix or superior cingulum white matter bundles. The eigenvalues taken separately add complementary information to the FA and Tr metrics and may be useful indices in better understanding the architectural reorganization of limbic system tracts in TLE patients without HS.

HIPPOCAMPAL SCLEROSIS (HS) is an entity of neuronal loss with gliosis involving the hippocampus and is the most common disease associated with intractable temporal lobe epilepsy (TLE). Conventional, anatomical magnetic resonance imaging (MRI) has been widely used for the detection of brain lesions that result in seizure activity. However, a major limitation of MRI is the fact that MRI studies can be completely normal in patients with TLE. By contrast, diffusion tensor imaging (DTI) is sensitive to physiological changes that take place in the brain tissue ictally and interictally.

The relevance of the limbic system as a neural circuitry to TLE is well recognized (1). The two most visible white matter connections in this circuit are the fornix, which projects from the hippocampus to the septal region and mamillary bodies, and the cingulum, which connects the entorhinal cortex and the cingulate gyrus.

As there is widespread propagation of synchronized neuronal firing in seizure disorders via neuronal networks, cortical and subcortical regions in the brain can be affected despite a single seizure focus (2,3). Therefore, evaluation of white matter tracts connecting these various regions may provide useful information regarding the diffuse changes in the brain that accompany TLE.

The integrity of the axonal microenvironment can be indirectly evaluated using DTI, which relies on measuring the diffusion of water and its directionality in three dimensions. Myelin sheaths that surround the axons may contribute to the anisotropy for both intra- and extracellular water (4). The most fundamental quantitative measures are the three eigenvalues $\lambda 1$, $\lambda 2$, and $\lambda 3$ of the diffusion tensor, which correspond to the principal diffusion coefficients measured either along the fiber tracts ($\lambda 1$) or perpendicular to them ($\lambda 2$, $\lambda 3$). The eigenvalues reflect the shape of the

ellipsoid and their sum (the trace) reflects the size of the ellipsoid. The most commonly used diffusion tensor indices are the trace (Tr) or the mean diffusivity (Tr/3) which characterizes the overall presence of obstacles to water diffusion, and the fractional anisotropy (FA), which is associated with the presence of oriented structures in tissue (5). In normal fiber tracts, water diffusion is anisotropic (ie, high FA), whereas in degenerated fibers the FA decreases substantially (6).

Brain fiber tractography using tensor diffusion data allows depiction of white matter tracts, and comparison between normal and diseased fiber tracts enables quantification of white matter changes due to damage (7,8).

Recent DTI studies focused on the axonal integrity of the fornix and cingulum in TLE patients with unilateral mesial temporal sclerosis (9,10). DTI abnormalities have also been demonstrated in several white matter tracts in adult patients with TLE, including in the internal capsule, the external capsule, the corpus callosum, the fornix and the cingulum (8,11). In TLE, it has been suggested that the epileptogenic zone is involved in a hyperexcitable network with extensive connections between the mesial temporal lobe structures, involving the temporal lobe and cingulate gyrus white matter (12).

DTI analysis in patients with partial seizures and a normal conventional MRI revealed significant differences in diffusion indices compared with the control group, suggesting that minor structural disorganization exists in occult epileptogenic cerebral lesions (13). TLE patients with and without HS also have distinctly different extratemporal white matter involvement. While some white matter bundles are affected equally in both forms of TLE, abnormalities of the bundles directly related to the mesial temporal structures appear to be unique to TLE patients with unilateral mesial temporal sclerosis (14,15). Thalamic abnormalities were detected in patients with or without HS and presented a bilateral gliosis or neuronal loss in both groups (16).

The purpose of this study was to identify the DTI parameters able to detect water diffusion abnormalities in the fornix, parahippocampal cingulum, and cingulate gyrus white matter fibers in TLE patients without HS (TLE−HS) and TLE patients with HS (TLE+HS) compared with healthy controls.

For the remainder of this article the parahippocampal cingulum fibers will be referred to as the inferior cingulum and the cingulum fibers near the cingulate gyrus will be referred to as the superior cingulum.

MATERIALS AND METHODS

Subjects

Eighteen patients with seizures localized in the temporal lobe were recruited and separated into two groups regarding the MR findings: nine TLE−HS patients (six females, three males, mean ± standard deviation [SD] age = 30.8 ± 10.1 years) with no evidence of signal abnormalities on conventional MRI and nine TLE+HS patients (seven females, two males, mean ± SD age = 33.0 ± 8.3 years). The patients and 10 control subjects (seven females, three males, mean ± SD age = 31.0 ± 5.4 years) without a history of neurological disease were scanned using DTI. Informed consent was obtained after the nature of the procedure had been fully explained before scanning.

After reviewing the patients' medical records the selection criteria were defined: 18–60 years of age, complex partial seizures of definite or probable temporal lobe origin, absence or presence of hippocampal sclerosis on MRI conventional data, and no other neurological disorder. The TLE diagnosis relied on electroclinical data, electroencephalograph (EEG) recording, and conventional MRI. The absence/presence of HS on conventional MR images allowed the separation of the patients into two groups: with and without HS.

Clinical and MRI patient data including the side of the epileptogenic focus are presented in Table 1.

MRI Technique

DT-MRI data were performed on a clinical 1.5T system (Sonata Siemens, Germany) with actively shielded magnetic field gradients (40 mT/m maximum amplitude).

Conventional MRI

The following MRI pulse sequences were acquired: T1-weighted images (TR = 430 msec, TE = 8 msec); T2-weighted fast spin echo (FSE) (TR = 6000 msec, TE = 102 msec); fluid attenuated inversion recovery (FLAIR) (TR = 8740 msec, TE = 104 msec, TI = 2200 msec).

DTI acquisition was performed by single-shot spin-echo echo planar imaging (EPI; TR = 5300 msec, TE = 110 msec, 240 × 240 mm^2 field of view [FOV], 128 × 128 acquisition matrix, 1.875 × 1.875 × 4 mm^3 nominal voxel size). Using a slice thickness of 4 mm without gap, 30 images were acquired through the entire brain. Diffusion-sensitizing gradient encoding was applied in 25 directions with a diffusion-weighted factor (b = 1000 s/mm^2), and the reference image was acquired without use of a diffusion gradient (b = 0 s/mm^2). The gradient directions were chosen using the technique described by Basser et al (17). Twenty-six images were obtained at each section, yielding total of 780 images. DTI images were acquired only on the axial plane. DTI acquisition time was ≈7 minutes per subject study.

Hippocampal MR Measurements

In order to confirm the qualitative findings on conventional MR images we conducted quantitative analysis of signal-to-noise ratio (SNR) on bilateral hippocampi in all subjects. Hippocampi were delineated in one plane where they are best visualized, avoiding the adjacent cerebrospinal fluid (CSF) space and the temporal white matter. Regions of interests (ROIs) were defined by standardized circular regions, each encompassing 49 pixels within each hippocampus on the T2-weighted EPI image (b = 0). The hippocampal

Table 1
Clinical and Conventional MRI Findings in TLE Patients

TLE patients no.	Age	Sex	Age at onset (years)	Duration (years)	EEG ictal	EEG interictal	Qualitative MRI (findings of hippocampal hypersignal on T2 images)		Hippocampal SNR measurements (z-score values)	
							Left	Right	Left	Right
1	26	F	5	21	_	LT	No	No	0.15	0.006
2	53	F	33	20	_	LT	No	No	0.10	0.2
3	19	F	8	11	LT	LT	No	No	1.19	1.08
4	34	F	1	33	LT	LT	No	No	1.33	1.68
5	35	F	18	17	LT	LT	No	No	1.33	1.51
6	36	M	15	21	RT	RT	No	No	−0.79	−0.51
7	26	M	22	4	LT	LT	No	No	−1.22	−1.10
8	23	M	17	6	_	LT	No	No	−0.62	−0.61
9	26	F	23	3	_	LT	No	No	−0.47	−0.33
10	42	F	7	35	RT	RT	No	Yes	0.72	3.88*
11	26	M	17	6	LT	LT	Yes	No	4.94*	0.09
12	45	F	10	35	LT	LT	Yes	No	2.83*	1.04
13	36	F	34	2	LT, F	LT	Yes	No	2.91*	0.63
14	26	M	9	17	LT	LT	Yes	No	3.36*	−1.30
15	22	F	17	5	LT	LT	Yes	No	7.02*	1.81
16	40	F	35	5	LT	LT	Yes	No	3.32*	−0.58
17	34	F	16	18	RT	RT	No	Yes	0.68	4.50*
18	26	F	20	6	LT	LT	Yes	No	5.13*	0.08

L = left; R = right; T = temporal; F = frontal; neg = no abnormalities detected. The asterisk (*) corresponds to abnormal Z-score ($P < 0.05$).

ROI's size was smaller than the measured structure in order to minimize the partial volume effects due to CSF sampling and possible head displacement during the scan.

The noise was estimated in a standardized circular ROI measuring 625 pixels, extracted from background (Fig. 1), paying attention to place it far from ghosting and filter artifacts, visible as an increased signal near image edges. SNR was calculated using the method described by Dietrich et al (18).
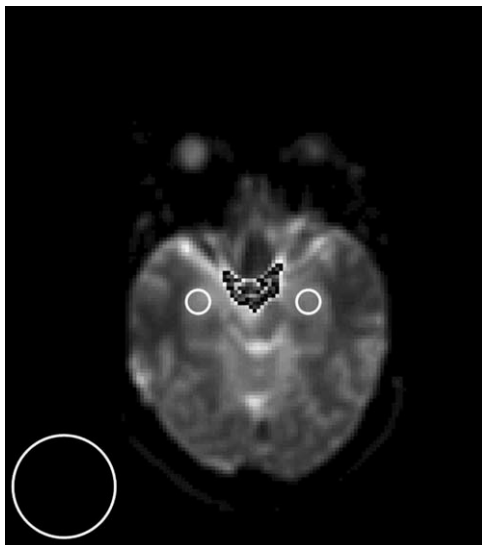
Figure 1. Left and right hippocampal ROIs (49 pixels) on a T2 (b = 0) axial slice for signal evaluation. At the bottom right of the image the ROI is positioned (625 pixels) for noise evaluation.

To identify SNR anomalies in single patients, the SNR of hippocampus was converted into Z-score using formula: SNR Z-score = (SNR$_{\text{patient hippocampus}}$ − Mean SNR$_{\text{controls}}$)/Standard Deviation SNR$_{\text{controls}}$.

The standardized Z-score was calculated for each patient, and included the hippocampal SNR subtracted by the mean and SD of the SNR values in control patients (Table 1).

Fibers Analysis

Tractography Method

The DTI images were processed on an independent workstation using MedInria 1.8.0 software (INRIA, Sofia Antipolis) (19). The software uses the tractography algorithm described by Mori et al (20) and Basser et al (21). The algorithm starts from a voxel center and proceeds in the direction of the major axis of the diffusion ellipsoid. When the edge of the voxel is reached, the direction is changed to that of the neighboring voxel. Propagation in each fiber tract was terminated if a voxel with an FA value less than 0.2 was reached or turned at an angle greater than 45°. This method was adapted and extended in the MedInria software (22). The criteria for judging local continuity include minimal FA value, local curvature (angle difference between consecutive vectors), and local coherence (regularization over local neighborhood). This method provides traces with subvoxel precision by using a concept similarly to the well-known surface extraction method based on marching cubes.

Tractography and subsequent measurements were performed separately for the left and right tract regions in each subject. Diffusion tensor measurements were obtained from the voxels that form the 3D
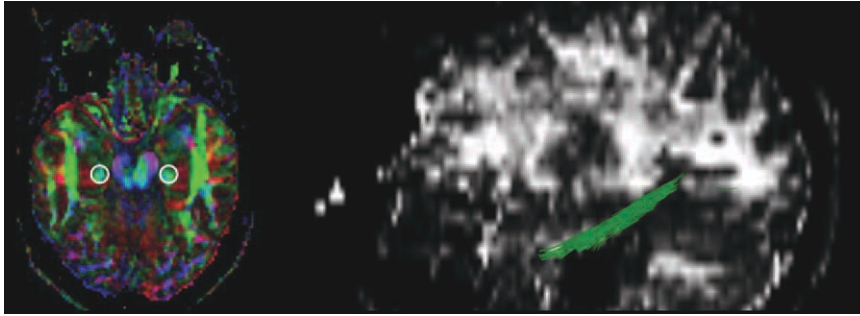
Figure 2. ROI placement for inferior cingulum tract selection. Color-coded maps were used to represent tract information. [Color figure can be viewed in the online issue, which is available at wileyonlinelibrary.com.]

structures derived from tractography, not from the ROIs used for tract selection.

Tract Selection

For the assessment of inferior cingulum and fornix, a seed ROI for tractography was drawn by a board-certified neuroradiologist on the axial slice where the tract could be identified on the b = 0 image. Each fiber tract was identified using unique or multiple ROIs to select a population of streamlines that followed the paths known from anatomy (23). Additional ROIs were used to either eliminate or truncate stray fibers that did not conform to a priori knowledge about the particular fiber tract. These manually assisted fiber-tracking procedures have been previously shown to be quite reliable, even for operators without previous fiber-tracking experience (24).

We computed full-brain tractography and then selected the tracts that run through the ROI. The software was used to create the FA color-coded map, and color-coded directionality maps of diffusion, which were overlaid on each other. The color-coded directional maps (red: left-to-right direction; green: anterior-to-posterior direction; blue: superior-to-inferior direction) provided easy visualization of the white matter fiber tracts.

The cingulum bundles are represented in two separate, cingulated (superior cingulum) and hippocampal (inferior cingulum) portions. This separation is done primarily because of the crossing fibers between the two portions of the tract making it difficult or impossible to generate streamlines tracing the entire cingulum with the deterministic tracking algorithm (25).

The inferior cingulum includes both long association fibers and shorter association fibers within the temporal lobe. In order to depict the inferior cingulum fibers, one ROI per tract located on the axial slice that provided the clearest view of the hippocampus was needed (Fig. 2).

For the superior cingulum fibers, two manual ROIs were drawn to adequately select the region: the first ROI was placed at the level of the border of the corpus callosum and a second ROI placed at the inferior border of the corpus callosum (Fig. 3).

The fornix originates in the hypothalamic area, and its anterior and posterior projections in the hypothalamus can be identified on the color map (Fig. 4). However, as the projection turned laterally and approached the hippocampus, the fornix–stria terminalis distinction became obscure at the current image resolution.

Based on the geometry of the tract visualized on the 2D axial slices we draw the ROIs as follows: On the inferior cingulum one circled ROI with size of ≈20 pixels was drawn; On the fornix and superior cingulum we draw two ellipsoid ROIs with a size of ≈12 pixels and 20 pixels, respectively.

The ROIs delineation was guided by the color-coded directional maps in order to avoid the neighboring fiber tracts voxels, especially in the case of fornix and superior cingulum.

Statistical Analysis

Statistical analysis was performed using STATISTICA 6.1 (StatSoft, Tulsa, OK) software.

The mean values of FA, Tr, $\lambda 1$, $\lambda 2$, and $\lambda 3$ and their SDs were calculated bilaterally for the fornix, inferior and superior cingulum of each subject group. Because no statistically significant differences were found in the control group between left and right DTI parameters in fornix (all $P > 0.78$), inferior cingulum (all $P > 0.78$), and superior cingulum (all $P > 0.48$), measurements were averaged to obtain a single value per individual (ie, [left + right]/2)).
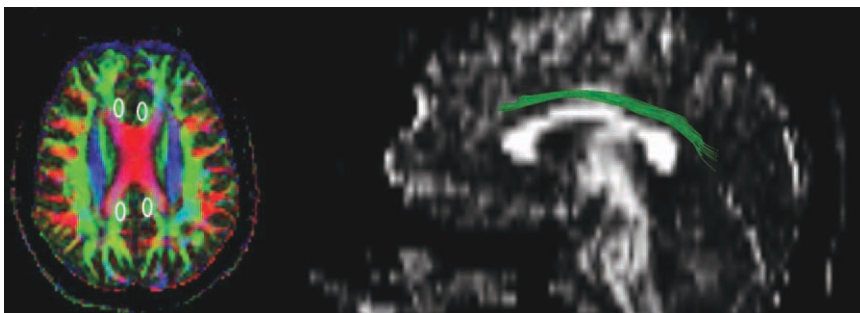
Figure 3. ROI placement for superior cingulum tract selection. Color-coded maps were used to represent tract information. [Color figure can be viewed in the online issue, which is available at wileyonlinelibrary.com.]

Figure 4. ROI placement for fornix tract selection. Color-coded maps were used to represent tract information. [Color figure can be viewed in the online issue, which is available at wileyonlinelibrary.com.]
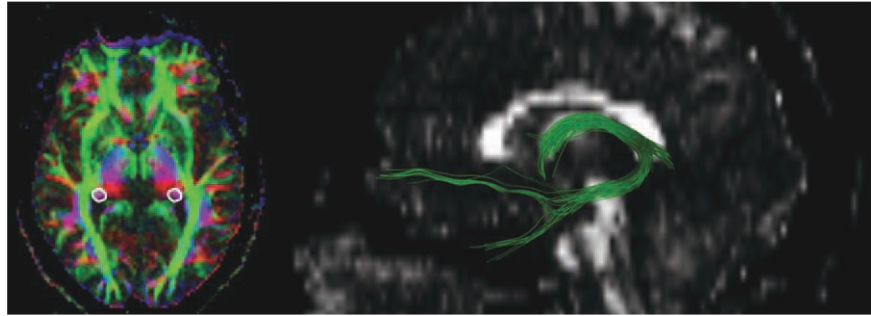
For patient groups, the left and right measurements were categorized into ipsilateral and contralateral to seizure side. Group comparisons were assessed using a two-tailed t-test.

The correlation of ipsilateral and contralateral to seizure side DTI parameters of the white matter bundles with age, age of seizure onset, and disease duration was examined using the Spearman rank correlation coefficient (r). Initially, $P < 0.05$ was considered statistically significant. A Bonferroni–Holm post-hoc correction was used to compensate for the family-wise error rate in multiple comparisons for each group of pairwise comparisons.

The inter- and intraobserver analysis was conducted on the inferior cingulum using Pearson's correlation coefficient (PCC).

RESULTS

There was no significant age difference between control and TLE−HS patients ($P = 0.97$), between control and TLE+HS patients ($P = 0.53$), and between the patient groups ($P = 0.64$).

No significant correlation was found between ipsilateral and contralateral DTI parameters and patients' age, age of seizure onset, and disease duration for the analyzed white matter bundles ($r < 0.40$, $P > 0.05$). A strong correlation (PCC >0.5) was found interobservers and intraobservers on the inferior cingulum.

Quantitative SNR analysis confirmed the qualitative MRI findings on the affected hippocampus, the difference between patients' mean SNRs hippocampus, and controls' mean SNR hippocampus being greater than two SDs of the controls mean SNR hippocampus (Table 1).

Ipsilateral DTI Parameters

Inferior Cingulum Fibers

We detected significantly different $\lambda 2$ ($P = 8.4 \times 10^{-3}$) and $\lambda 3$ ($P = 6.3 \times 10^{-4}$) (increased) values in the ipsilateral inferior cingulum fibers between controls and TLE−HS patients (Table 2). No significant differences were found between controls and this patient group for $\lambda 1$ ($P = 0.61$) and Tr ($P = 0.07$). All TLE−HS patients presented a statistically significantly different (decreased) FA on the inferior cingulum ipsilateral to the seizure side (Table 2) compared with controls ($P = 2.8 \times 10^{-5}$).

The TLE+HS patients group showed significantly different abnormalities characterized by increased $\lambda 2$ ($P = 1.9 \times 10^{-5}$), $\lambda 3$ ($P = 1.1 \times 10^{-7}$), and Tr ($P = 1.3 \times 10^{-4}$), and decreased FA ($P = 2.2 \times 10^{-6}$), when compared with controls. No significant differences were detected between HS patients and controls in $\lambda 1$ ($P = 0.24$).

Fornix Fibers

In TLE−HS patients, increased $\lambda 3$ and decreased FA values were found statistically significant when comparing with controls ($P = 0.009$ and $P = 0.001$, respectively). In the TLE+HS group, we found increased $\lambda 2$ ($P = 5.8 \times 10^{-3}$) and $\lambda 3$ ($P = 5.9 \times 10^{-3}$), and decreased FA ($P = 5.3 \times 10^{-4}$), compared with controls (Table 2).

Superior Cingulum Fibers

Compared with controls, only the FA parameter was found to be statistically significant (decreased) ($P = 1.7 \times 10^{-3}$) and was found in superior cingulum ipsilateral to epileptogenic zone in the TLE−HS patient group (Table 2). Comparisons between TLE+HS patients and controls showed statistically significant (increased) $\lambda 3$ ($P = 2.2 \times 10^{-4}$) and (decreased) FA ($P = 1.3 \times 10^{-5}$).

Contralateral DTI Parameters

No DTI parameters were found statistically significant when comparing the TLE−HS patient group with the control group in all tracts (Table 3) ($P > 0.05$). The $\lambda 2$ parameter was significantly different (increased) in inferior cingulum ($P = 3.7 \times 10^{-3}$) and in fornix ($P = 7 \times 10^{-3}$) in TLE+HS patients versus controls. Statistically increased $\lambda 3$ ($P < 0.004$) and decreased FA ($P < 0.003$) were found in all three tracts of TLE+HS patients when compared with controls.

DISCUSSION

We focused our study on fornix and cingulum white matter tracts since they are the major pathways involved in the epileptic network in TLE patients. By using DTI in combination with tractography we subdivided the cingulum fibers into two regions in order to selectively study their water diffusion properties in TLE patients.

Table 2
Mean and SD Values of Ipsilateral DTI Parameters in Fornix, Inferior and Superior Cingulum Fibers of TLE Patients and Controls

DTI indices	Ipsilateral inferior cingulum			Ipsilateral fornix			Ipsilateral superior cingulum		
	Controls	TLE-HS patients	TLE+HS patients	Controls	TLE-HS patients	TLE+HS patients	Controls	TLE-HS patients	TLE+HS patients
FA	0.41 ± 0.01	$0.35 \pm 0.03^*$	$0.33 \pm 0.03^*$	0.43 ± 0.01	$0.40 \pm 0.02^*$	$0.40 \pm 0.02^*$	0.46 ± 0.02	$0.42 \pm 0.03^*$	$0.41 \pm 0.01^*$
Tr ($\times10^{-3}$ mm^2/s)	2.48 ± 0.13	2.61 ± 0.15	$2.74 \pm 0.09^*$	2.48 ± 0.10	2.59 ± 0.17	2.65 ± 0.17	2.13 ± 0.11	2.15 ± 0.09	2.22 ± 0.07
$\lambda 1$ ($\times10^{-3}$ mm^2/s)	1.22 ± 0.07	1.21 ± 0.05	1.26 ± 0.05	1.23 ± 0.05	1.25 ± 0.08	1.27 ± 0.07	1.08 ± 0.05	1.06 ± 0.03	1.09 ± 0.03
$\lambda 2$ ($\times10^{-3}$ mm^2/s)	0.73 ± 0.03	$0.79 \pm 0.05^*$	$0.82 \pm 0.04^*$	0.74 ± 0.03	0.78 ± 0.05	$0.80 \pm 0.06^*$	0.64 ± 0.04	0.65 ± 0.03	0.68 ± 0.02
$\lambda 3$ ($\times10^{-3}$ mm^2/s)	0.53 ± 0.03	$0.61 \pm 0.05^*$	$0.66 \pm 0.04^*$	0.51 ± 0.03	$0.56 \pm 0.05^*$	$0.57 \pm 0.06^*$	0.41 ± 0.03	0.44 ± 0.04	$0.46 \pm 0.02^*$

*$P < 0.05$, Bonferroni-Holm corrected between controls and patient groups. No significant differences were found between patient groups.

Table 3
Mean and SD Values of Contralateral DTI Parameters in Fornix, Inferior and Superior Cingulum Fibers of TLE Patients and Controls

DTI indices	Contralateral inferior cingulum			Contralateral fornix			Contralateral superior cingulum		
	Controls	TLE-HS patients	TLE+HS patients	Controls	TLE-HS patients	TLE+HS patients	Controls	TLE-HS patients	TLE+HS patients
FA	0.41 ± 0.01	$0.41 \pm 0.03\uparrow$	$0.34 \pm 0.04^*$	0.43 ± 0.01	0.41 ± 0.02	$0.40 \pm 0.02^*$	0.46 ± 0.02	0.45 ± 0.02	$0.43 \pm 0.01^*$
Tr ($\times10^{-3}$ mm^2/s)	2.48 ± 0.13	$2.29 \pm 0.09\uparrow$	2.61 ± 0.15	2.48 ± 0.10	2.52 ± 0.13	2.61 ± 0.13	2.13 ± 0.11	2.16 ± 0.07	2.21 ± 0.08
$\lambda 1$ ($\times10^{-3}$ mm^2/s)	1.22 ± 0.07	1.18 ± 0.04	1.20 ± 0.06	1.23 ± 0.05	1.23 ± 0.07	1.26 ± 0.05	1.08 ± 0.05	1.05 ± 0.04	1.10 ± 0.03
$\lambda 2$ ($\times10^{-3}$ mm^2/s)	0.73 ± 0.03	$0.70 \pm 0.04\uparrow$	$0.79 \pm 0.05^*$	0.74 ± 0.03	0.75 ± 0.04	$0.79 \pm 0.04^*$	0.64 ± 0.04	0.67 ± 0.03	0.67 ± 0.03
$\lambda 3$ ($\times10^{-3}$ mm^2/s)	0.53 ± 0.03	$0.52 \pm 0.04\uparrow$	$0.61 \pm 0.06^*$	0.51 ± 0.03	0.53 ± 0.04	$0.56 \pm 0.04^*$	0.41 ± 0.03	0.44 ± 0.03	$0.44 \pm 0.02^*$

*$P < 0.05$, Bonferroni-Holm corrected between controls and patient groups.

It has been suggested that the analysis of the full diffusion tensor including eigenvalues can provide information on structural integrity and the underlying histological processes following injury to cerebral white matter (26).

The major finding of this study was that different patterns of diffusion changes found in TLE−HS and TLE+HS patients imply that, between all three investigated tracts, the inferior cingulum seems to be the most affected in terms of DTI abnormalities.

An interesting finding was that both patient groups presented normal $\lambda1$, increased $\lambda2$ and $\lambda3$, and decreased FA in inferior cingulum when compared with controls. Examination of the eigenvalues yields interesting and clinically relevant information on the underlying causes of reduced anisotropy. It has been suggested the $\lambda1$ parameter reflects axonal disruption in white matter fibers, while diffusivities perpendicular to the fibers ($\lambda2$ and $\lambda3$) may indicate myelin degradation (27).

Normally, axonal membranes and myelin pose barriers to water displacement, such that water preferentially diffuses along the direction of the axons (28). As axons degenerate and break down with subsequent degradation of myelin, the barriers that normally hinder the diffusion of water across the axons disappear, allowing a more spatially uniform profile of water displacement (ie, isotropic diffusion) (29).

While similar increases in $\lambda2$ and $\lambda3$ and reductions in FA were observed in both patient groups, in TLE+HS patients the structural disorganization and slight expansion of the extracellular space were detected by DTI as an area of increased trace in inferior cingulum. Our findings are in agreement with those reported by Concha et al (10), characterized by increased mean diffusivity (Tr/3) and reduced FA. It has been suggested that increased trace reflects reduced cellular density or extracellular edema possibly due to increased membrane permeability (30).

In TLE−HS patients, the reduced FA associated with a normal mean diffusivity suggests a loss of directional organization in combination with a preserved cells density (31). The normal trace found in inferior cingulum fibers of TLE−HS patients is supported by the results reported by Shon et al (14), which used a voxel-based method to identify DTI abnormalities while we evaluated DTI changes using a tractography method.

On the contralateral to seizure side, no diffusion changes were detected, suggesting that in inferior cingulum of TLE−HS patients the seizure network may not be extensive. However, in the TLE+HS group findings in inferior cingulum parameters are similar to those reported by Concha et al (10).

In addition to a significantly reduced FA found in both patient groups, by analyzing the perpendicular diffusivities separately (without averaging them), we have shown a significant increase in $\lambda2$ and $\lambda3$ in fornix of TLE+HS and only $\lambda3$ in fornix of TLE−HS. The fornix is a heterogeneous structure containing bidirectional fibers interconnecting multiple brain regions. Our results suggest that the diffusion changes are primarily in the direction perpendicular to the axons and are similar to the data reported by Concha et al (15). These changes are consistent with axonal degeneration within the fiber tract. Based on our findings, we may consider that in fornix fibers of TLE−HS patients there is a structural modification of axonal membrane probably expressing a myelin degradation beginning (27), not yet visible on the MR conventional images. As Govindan et al (32) observed, the $\lambda3$ analyzed separately seems to be the most robust parameter in the presence of crossing fibers within the voxels.

On the contralateral side of TLE+HS patients, we observed the same DTI abnormal changes—increased $\lambda2$ and $\lambda3$, normal $\lambda1$ and Tr, and reduced FA—as in the ipsilateral side. These findings are consistent with axonal degeneration within the fiber tract (10,31).

The superior cingulum of TLE+HS patients showed an increased $\lambda3$ and decreased FA. These findings were detected bilaterally in the TLE+HS patient group, supporting the idea that HS is associated with bilateral limbic system pathology (10). The same DTI pattern was observed in the fornix of the TLE−HS patient group and control patients.

In TLE−HS patients, $\lambda1$, $\lambda2$, and $\lambda3$ values did not reach statistical significance when compared with controls. This observation might suggest that there is no modification in water molecule displacements.

The TLE−HS patients showed only a reduced FA in the superior cingulum, suggesting the presence of fiber loss due to axonal membrane breakdown (6). This finding is in agreement with the results of Concha et al (15) that showed decreased anisotropy in white matter tracts such as the cingulum and fornix of TLE−HS patients.

In all ipsilaterally investigated white matter tracts, the DTI parameters failed to significantly differentiate the two patient groups. The FA parameter changes appear to be less sensitive to structural changes causing loss of tissue organization in TLE patient groups. Alternatively, different pathophysiological mechanisms could be responsible for the differences between the two TLE patient groups (33).

Further studies implicating a higher number of TLE patients with normal conventional MRI and correlation of tractography with clinical information would be interesting to reinforce our study and to determine the role of tractography in diagnostic accuracy of TLE patients.

In conclusion, our findings suggest that, depending on the white matter fiber localization with regard to epileptogenic zone, the limbic system tracts have a different DTI pattern in TLE patients with and without HS. Using white matter tractography combined with DTI in both patient groups we may suggest that the inferior cingulum tract has more water diffusion changes than the two other analyzed tracts. The eigenvalues analyzed separately depict different structural abnormalities in limbic system tracts of TLE patients with no abnormalities on conventional MRI. Our DTI findings not detected with conventional MRI that correlated with the EEG epileptogenic side, may be considered an integral component of pretherapeutic evaluation that may have an impact on surgical strategy.

REFERENCES

1. Kuzniecky R, Bilir E, Gilliam F, Faught E, Martin R, Hugg J. Quantitative MRI in temporal lobe epilepsy: evidence for fornix atrophy. Neurology 1999;53:496–501.

2. Thivard L, Lehericy S, Krainik A, et al. Diffusion tensor imaging in medial temporal lobe epilepsy with hippocampal sclerosis. Neuroimage 2005;28:682–690.

3. Kimiwada T, Juhász C, Makki M, et al. Hippocampal and thalamic diffusion abnormalities in children with temporal lobe epilepsy. Epilepsia 2006;47:167–175.

4. Beaulieu C. The basis of anisotropic water diffusion in the nervous system. NMR Biomed 2002;15:435–455.

5. Basser PJ, Pierpaoli C. Microstructural and physiological features of tissues elucidated by quantitative diffusion tensor MRI. J Magn Reson B 1996;111:209–211.

6. Beaulieu C, Does MD, Snyder RE, Allen PS. Changes in water diffusion due to Wallerian degeneration in peripheral nerve. Magn Reson Med 1996;36:627–631.

7. Mori S, van Zijl PC. Fiber tracking: principles and strategies — a technical review. NMR Biomed 2002;15:468–480.

8. Gross DW, Concha L, Beaulieu C. Extratemporal white matter abnormalities in mesial temporal lobe epilepsy demonstrated with diffusion tensor imaging. Epilepsia 2006;47:1360–1363.

9. McDonald CR, Ahmadi ME, Hagler DJ, et al. Diffusion tensor imaging correlates of memory and language impairments in temporal lobe epilepsy. Neurology 2008;71:1869–1876.

10. Concha L, Beaulieu C, Gross DW. Bilateral limbic diffusion abnormalities in unilateral temporal lobe epilepsy. Ann Neurol 2005;57: 188–196.

11. Arfanakis K, Hermann BP, Rogers BP, Carew JD, Seidenberg M, Meyerand ME. Diffusion tensor MRI in temporal lobe epilepsy. Magn Reson Imaging 2002;20:511–519.

12. Bertram EH, Zhang DX, Mangan P, Fountain N, Rempe D. Functional anatomy of limbic epilepsy: a proposal for central synchronization of a diffusely hyperexcitable network. Epilepsy Res 1998;32:194–205.

13. Rugg-Gunn FJ, Eriksonn SH, Symms MR, Barker GJ, Duncan JS. Diffusion tensor imaging of cryptogenic and acquired partial epilepsies. Brain 2001;124:627–636.

14. Shon YM, Kim YI, Koo BB, et al. Group-specific regional white matter abnormality revealed in diffusion tensor imaging of medial temporal lobe epilepsy without hippocampal sclerosis. Epilepsia 2010;51:529–535.

15. Concha L, Beaulieu C, Collins DL, Gross DW. White-matter diffusion abnormalities in temporal-lobe epilepsy with and without mesial temporal sclerosis. J Neurol Neurosurg Psychiatry 2009;80:312–319.

16. Kim CH, Koo BB, Chung CK, Lee JM, Kim JS, Lee SK. Thalamic changes in temporal lobe epilepsy with and without hippocampal sclerosis: a diffusion tensor imaging study. Epilepsy Res 2010;90: 21–27.

17. Basser PJ, Mattiello J, Le Bihan D. MR diffusion tensor spectroscopy and imaging. Biophys J 1994;66:259–267.

18. Dietrich O, Raya JG, Reeder SB, Reiser MF, Schoenberg SO. Measurement of signal-to-noise ratios in MR images: influence of multichannel coils, parallel imaging, and reconstruction filters. J Magn Reson Imaging 2002;26:375–385.

19. http://www–sop.inria.fr/asclepios/software/MedINRIA/

20. Mori S, Crain BJ, Chacko VP, van Zijl PCM. Three-dimensional tracking of axonal projections in the brain by magnetic resonance imaging. Ann Neurol 1999;45:265–269.

21. Basser BJ, Pajevic S, Pierpaoli C, Duda J, Aldroubi A. In vivo fiber tractography using DT-MRI data. Magn Reson Med 2000; 44:625–632.

22. Fillard P, Gerig G. Analysis tool for diffusion tensor MR. In: Proc MICCAI'03, Part II, volume 2879 of LNCS, November 2003. p 979–980.

23. Wakana S, Jiang H, Nagae-Poetscher LM, van Zijl PC, Mori S. Fiber tract-based atlas of human white matter anatomy. Radiology 2004;230:77–87.

24. Wakana S, Caprihan A, Panzenboeck MM, et al. Reproducibility of quantitative tractography methods applied to cerebral white matter. Neuroimage. 2007;36:630–644.

25. Hagler DJ Jr, Ahmadi ME, Kuperman J, et al. Automated white-matter tractography using a probabilistic diffusion tensor atlas: application to temporal lobe epilepsy. Hum Brain Mapp 2009;30: 1535–1547.

26. Concha L, Gross DW, Wheatley M, Beaulieu C. Diffusion tensor imaging of time-dependent axonal and myelin degradation after corpus callosotomy in epilepsy patients. Neuroimage 2006;32: 1090–1099.

27. Budde MD, Kim JH, Liang HF, et al. Toward accurate diagnosis of white matter pathology using diffusion tensor imaging. Magn Reson Med 2007;57:688–695.

28. Beaulieu C. The basis of anisotropic water diffusion in the nervous system — a technical review. NMR Biomed 2002;15:435–455.

29. Beaulieu C, Does MD, Snyder RE, Allen PS. 1996. Changes in water diffusion due to Wallerian degeneration in peripheral nerve. Magn Reson Med 1996;36:627–631.

30. Gass A, Niendorf T, Hirsch JG. Acute and chronic changes of the apparent diffusion coefficient in neurological disorders — biophysical mechanisms and possible underlying histopathology. J Neurol Sci 2001;186:15–23.

31. Wieshmann UC, Clark CA, Symms MR, Barker GJ, Birnie KD, Shorvon SD. Water diffusion in the human hippocampus epilepsy. Magn Reson Imaging 1999;17:29–36.

32. Govindan RM, Makki MI, Sundaram SK, Juhász C, Chugani HT. Diffusion tensor analysis of temporal and extra-temporal lobe tracts in temporal lobe epilepsy. Epilepsy Res 2008;80:30–41.

33. Carne RP, O'Brien TJ, Kilpatrick CJ, et al. TLE-HS PET-positive temporal lobe epilepsy: a distinct surgically remediable syndrome. Brain 2004;127:2276–2285.